JOURNAL OF PROPULSION AND POWER
Vol. 15, No. 2, March–April 1999

Annular Vane Swirler Performance

David G. Lilley*
Oklahoma State University, Stillwater, Oklahoma 74078

The flowfield immediately downstream of an annular vane swirler is investigated to aid in computer modeling of flowfields, and in the development and evaluation of turbulence models for swirling confined flow. The swirler studied is annular with a hub-to-swirler diameter ratio of 0.25, and 10 adjustable flat untwisted vanes with a pitch-to-chord ratio of 0.68. Measurements of time-mean axial, radial, and swirl velocities are made at the swirler exit plane, using a five-hole pitot probe technique with computer data reduction. The time-mean velocity components measured at the swirler exit plane show clearly the effects of centrifugal forces, recirculation zones, and blade wakes on the exit-plane velocity profiles. Nonaxisymmetry is present in all swirl cases investigated. Assumptions of flat axial and swirl profiles are found to be progressively less realistic as the swirl vane angle increases, with axial and swirl velocities peaking strongly at the outer edges of the swirler exit and significant nonzero radial velocities present.

Nomenclature

c = blade chord width
D = test section diameter
d = swirler exit diameter, $D/2$
G = axial flux of momentum
p = time-mean pressure
S = swirl number, $G_\theta/(G_x d/2)$
s = blade spacing or pitch
u, v, w = axial, radial, and swirl components of velocity
x, r, θ = axial, radial, and azimuthal cylindrical polar coordinates
θ = azimuth angle
ρ = density
ϕ = swirl vane angle

Subscripts
h = hub
in = inlet conditions, upstream of swirler
x = axial direction
θ = swirl direction
∞ = reference value at edge of swirler exit

Superscript
$'$ = alternate form, neglecting pressure variation; fluctuating quantity time-mean quantity

Introduction

A MORE complete understanding of the internal flowfield in combustion equipment has long been recognized as a need by designers. Various textbooks describe and discuss pertinent issues.[1–7] The present contribution concentrates on the time-mean flow characteristics being generated by the upstream annular swirler, using a five-hole pitot probe technique.

Research has progressed in several areas related to swirling flowfields, with flow visualization, pitot probe, and hot-wire measurements, and associated computer simulation and turbulence modeling studies. Lilley[8] reviews the studies related to axisymmetric flowfields, and Lilley[9] reviews the studies related to one and two laterally injected jets into the flowfield. Accuracy of predictions from a computer model is strongly dependent on the inlet boundary conditions used, which are primarily determined by the swirler and its performance at different vane angle settings.

In the present study, the main objective is to make time-mean velocity measurements as close as possible to the swirler exit, to define more accurately the performance characteristics of the swirler. A range of swirl-blade angles ϕ from 0 to 70 deg is considered, under low-speed, low-turbulence intensity conditions.

Theoretical Analysis

Idealized Velocity Profiles

All theoretical analyses of swirler performance and most numerical simulations of furnace flowfields have used simple idealized swirler exit velocity profiles. Common assumptions that are made include flat axial and swirl velocity profiles downstream of the swirler for swirlers with vanes of constant angle, and a flat axial profile with a linear swirl profile (solid-body rotation) for swirlers with helicoidal vanes and for tangential-entry swirl generators. These, however, have been found to be quite unrealistic.[10–14] The use of idealized profiles is also unwise when used as inlet conditions to a computer prediction of the combustor flowfield downstream of the inlet swirler.[8,15,16] The best remedy for numerical simulations is to use experimentally measured swirler exit profiles, if they are available.

Definition of Swirl Parameters

The swirl number is a nondimensional parameter used to characterize the degree of swirl generated by a swirler. It is defined as

$$s = \frac{G_\theta}{G_x(d/2)} \tag{1}$$

where the axial flux of angular momentum G_θ is given by

$$G_\theta = \int_0^{2\pi} \mathrm{d}\theta \int_0^{d/2} (\rho uw + \overline{\rho u'w'}) r^2 \, \mathrm{d}r \tag{2}$$

and the axial flux of axial momentum G_x is given by

$$G_x = \int_0^{2\pi} \mathrm{d}\theta \int_0^{d/2} [\rho u^2 + \overline{\rho u'^2} + (p - p_\infty)] r \, \mathrm{d}r \tag{3}$$

Received May 5, 1997; revision received Nov. 16, 1998; accepted for publication Nov. 16, 1998.

*Professor, School of Mechanical and Aerospace Engineering. Fellow AIAA.

and $d/2$ is the swirler exit radius. These equations are obtained from appropriate manipulation of the axial and azimuthal momentum equations, respectively. If the pressure term is omitted from the axial momentum, the dynamic axial momentum flux G_x' is obtained. This leads to an alternate definition of swirl number:

$$S' = \frac{G_\theta}{G_x' d/2} \tag{4}$$

Experimental Equipment and Procedure

Facility

A low-speed wind tunnel designed and built at Oklahoma State University has been used for all of the test measurements. It produces uniform flow of relatively low-turbulence intensity, with a continuously adjustable flow rate. The facility consists of a filtered intake, an axial blower, a stilling chamber, a turbulence management section, and a contoured outlet nozzle. It is described at length in Lilley.[8] The contoured nozzle is made of molded fiberglass with a steel flange at the outlet for the attachment of the swirler and/or expansion block en route to the test section in associated studies. A 1-cm-diam hole, located a short distance upstream of the outlet, allows for insertion of a standard pitot–static probe to measure the dynamic pressure upstream of the swirler. This measurement, with a small correction for difference in flow area, is used to calculate the swirler inlet reference velocity u_{in}. More information about this characteristic velocity used for velocity normalization is given with the results.

Swirler

The swirler used in this study is annular, with hub and housing diameters of 3.75 and 15.0 cm, respectively, giving a hub-to-swirler diameter ratio of 0.25. The hub has a streamlined parabolic nose facing upstream and a blunt base (corner radius ~2 mm) facing downstream. It is supported by four thin rectangular-sectioned struts or spider arms from the housing wall. The base of the hub protrudes ~3 mm downstream of the swirler exit plane. A schematic of the swirler is shown in Fig. 1, with 10 flat untwisted vanes or blades. The flat vane planform is shown in Fig. 2, and it may be noted that each of the 10 flat untwisted blades has a material thickness of ~1 mm. The 10 vanes or blades are attached to shafts that pass through the housing wall and allow individual adjustment of each blade's angle. The standard vanes are wedge shaped to give a constant pitch-to-chord ratio of 0.68, which according to two-dimensional cascade data, provide reasonably good flow-turning effectiveness.

Measurement Procedure

The time-mean velocity components are measured with a five-hole pitot probe that allows determination of the magnitude and direction of the mean velocity vector simultaneously. The probe is mounted in a traversing mechanism, which allows it to be translated vertically (on a radial line outward from the test section axis) and rotated about the probe's yaw axis. In addition to the motion permitted by the traverse mechanism, the test section tube on which the traverse mechanism is mounted may be rotated about its axis with respect to the swirler, thereby allowing azimuthal traverses to be performed. Tubing from the probe's five pressure taps is routed through selector valves to a differential pressure transducer, and the resulting pressure difference values are read directly from an integrating digital voltmeter. The pressure data are reduced by a computer program to yield nondimensionalized u, v, and w velocity components.

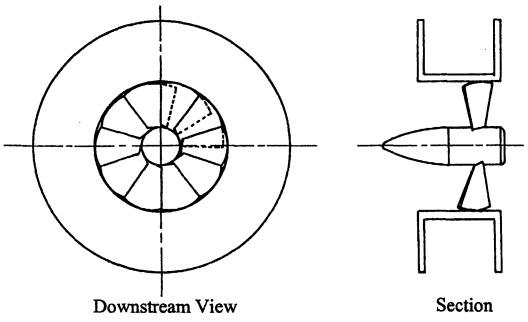

Fig. 1 Diagram of swirler, section and downstream view.

Experimental Results

The radial traverses consist of 10 points from the centerline to the swirler exit radius, spaced 7.6 mm apart. Of these 10, only seven stations were actually measured because the hub blocked the inner three positions. The azimuthal traverses contain nine points spaced 6 deg apart at a constant radial distance from the centerline. Azimuth angles θ were taken from -24 to $+24$ deg, with the $\theta = 0$ position in line with the shaft of one of the swirl vanes. A diagram showing the traverse patterns on the face of the swirler is given in Fig. 3. All traverses are taken immediately after the swirler exit downstream flange face, with a 90-deg flow expansion into the cylindrical test section, linear expansion ratio 2:1 (area expansion raio 4:1). The outer test section tube of diameter $D = 30$ cm and length 150 cm was present during all of the swirler exit flow measurements.

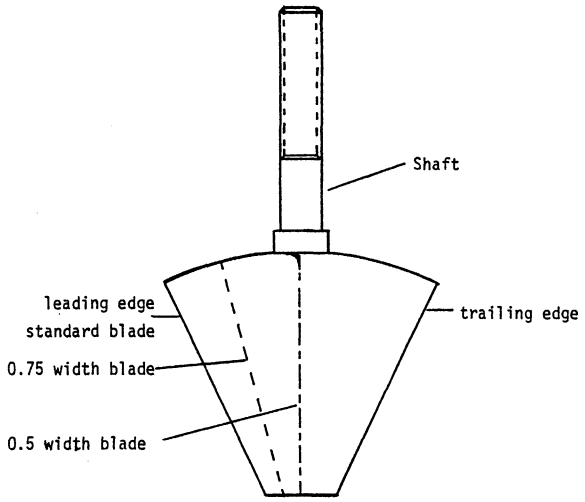

Fig. 2 Swirl vanes.

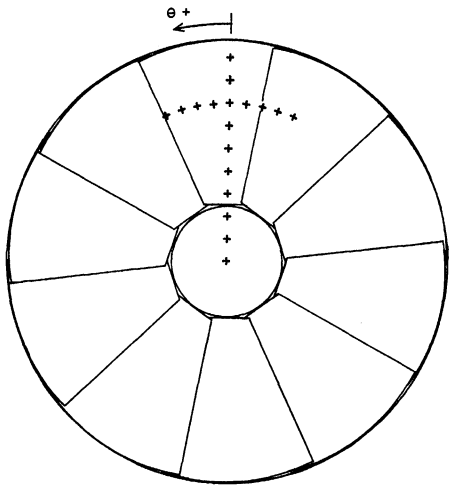

Fig. 3 Measurement locations, radial and azimuthal traverses.

Velocity Profiles from Radial Traverses

Radial traverses of axial, radial, and swirl velocity component data are presented for five values of swirl blade angle: zero (no swirler), and zero (with swirler), 38, 45, 60, and 70 deg, in Figs. 4–9, respectively, with the profiles extending from the centerline to twice the swirler blade region exit radius (r/D = 0.5, where D is the test section diameter used in associated studies). Note that r/D = 0.25 is the radial location of the outer swirler housing into which the blades are attached. This outer housing also has a flat flange attached at the downstream end of the swirler, covering the radial region from r/D = 0.25 to 0.5.

All velocities shown are normalized with respect to the swirler inlet uniform axial velocity u_{in}, deduced independently from the pitot–static measurement upstream of the swirler. This velocity is the uniform velocity that would occupy the round

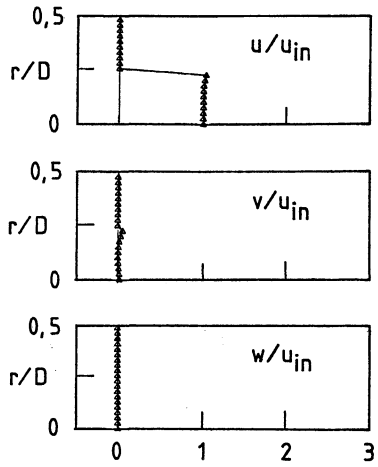

Fig. 4 Normalized velocity profiles from radial traverse, ϕ = 0 deg (no swirler).

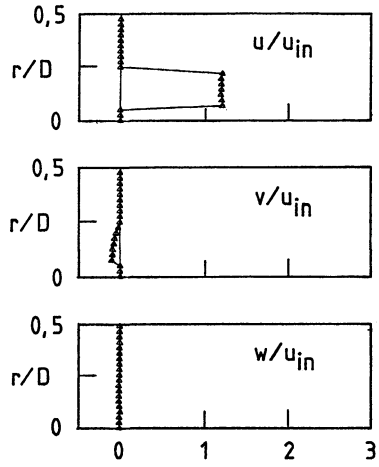

Fig. 5 Normalized velocity profiles from radial traverse, ϕ = 0 deg (swirler installed).

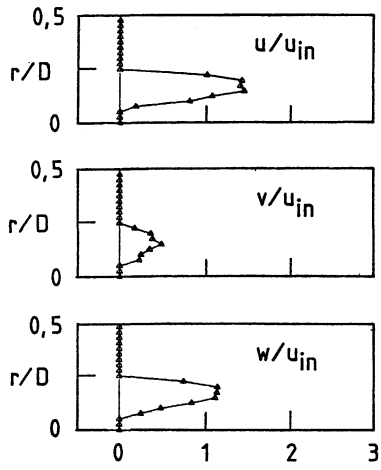

Fig. 6 Normalized velocity profiles from radial traverse, ϕ = 38 deg.

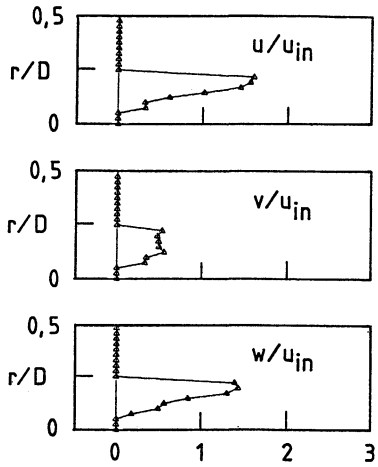

Fig. 7 Normalized velocity profiles from radial traverse, ϕ = 45 deg.

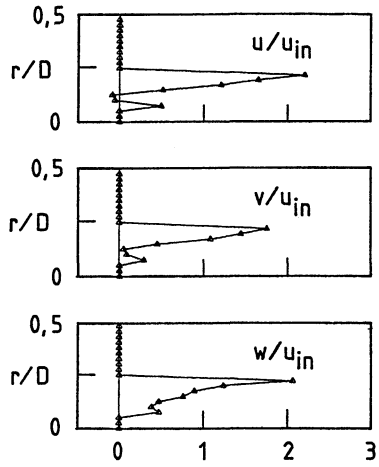

Fig. 8 Normalized velocity profiles from radial traverse, ϕ = 60 deg.

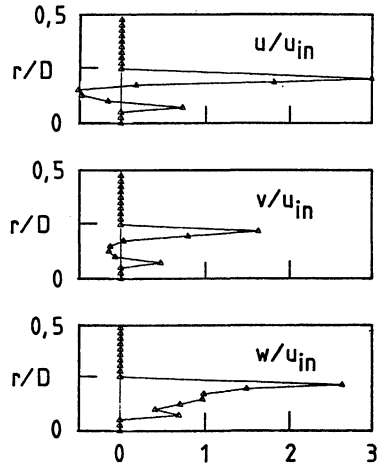

Fig. 9 Normalized velocity profiles from radial traverse, ϕ = 70 deg.

cross-sectional passageway in the absence of the swirler (see Fig. 4). When the swirler is present with swirl vane angle zero, the central hub of the swirler provides an axial velocity speed up, as seen in Fig. 5. Then, measurements are taken in the annular region between the outer extent of the hub and the inner extent of the swirler housing, where the spatially averaged axial velocity at this axial location is larger than u_{in}. The measuring plane is slightly downstream of the swirler blades themselves, and progressively so as the blade angles are increased, as may be deduced from Figs. 1 and 2.

The nonswirling case shown in Fig. 4 has a nearly flat axial velocity profile, as expected for the plain nozzle opening without the swirler installed. There is no measurable swirl velocity, and the radial velocity is zero except for points very near the edge of the exit, where the flow begins to anticipate the abrupt expansion to twice the exit diameter. The second nonswirling case (Fig. 5), has the swirler installed with the blades set to $\phi = 0$ deg. The traverse was made midway between two blades and away from any of the hub-supporting struts. Here again, the axial profile is quite flat, with just a slight increase toward the hub. However, the velocity has increased by nearly 25%, because of the decrease in flow area with swirler hub and vanes in place. In addition, the hub induces a negative radial velocity across the entire annulus, overriding the tendency to anticipate the expansion corner. The swirl velocity is, as expected, negligible.

The 38-deg blade-angle case in Fig. 6 shows remnants of the flat inlet profile over a small portion of the radius near the outside edge in both the axial and swirl profiles. The presence of the hub now constrains the three innermost points to zero, and the region between the hub and the flat portion in the axial and swirl profiles is approximately linear. The maximum axial velocity is 1.5 times the inlet axial velocity because the flow area is decreased by the hub, and also because centrifugal effects have shifted the profile outward. The radial velocity has an irregular profile with a maximum value of one-half the inlet axial velocity.

In the $\phi = 45$-deg case of Fig. 7, the flat segments are no longer present, and both axial and swirl profiles vary from zero at the hub to a maximum at or near the rim of the swirler in an almost linear fashion. The similar shape and magnitude of the profiles indicates that the turning angle is fairly uniform and only slightly less than 45 deg. The radial velocity is again irregular, but shows a step at $r/D = 0.1$ similar to that in the axial and swirl profiles; this is probably because of the central recirculation zone downstream beginning to slow down the flow upstream of it.

Profiles ensuing from the case of $\phi = 60$ deg (see Fig. 8), all have a sharply peaked shape, with most of the flow leaving near the outer boundary. The radial component is considerably stronger, with a peak value nearly twice that of the reference velocity upstream of the swirler. The step seen previously in the 45-deg axial profile has now developed into reverse flow, indicating that the central recirculation zone now extends upstream past the exit plane. The reverse flow is accompanied by reduced swirl velocity and very low values of radial velocity. The positive axial velocity adjacent to the hub may be the result of a slight clearance between the blades and the hub, allowing air with greater axial momentum to pass through.

Exit velocity profiles obtained for the strongest swirl case considered ($\phi = 70$ deg) are shown in Fig. 9. Almost all of the flow leaves the swirler at the outside edge. The maximum axial and swirl velocities are ~3 and 2.5 times the upstream reference values, respectively, and the velocity gradients across the profiles are quite large. The reverse flow in the center of the axial profile is stronger than in the 60-deg case, and is now accompanied by negative or inward radial velocity. This suggests the possibility of a vortex ring structure occurring at the exit of the swirler under high-swirl conditions. The swirl velocity profile remains positive, but shows a step corresponding to the outer boundary of the recirculation zone.

Table 1 Measured swirl numbers

ϕ	S	S'	w_{m0}/u_{m0}
38	0.567	0.559	0.801
45	0.765	0.718	0.876
60	0.850	0.759	0.937
70	0.883	0.750	0.887

Velocity Profiles from Azimuthal Traverses

An indication of the azimuthal or θ variation of axial, radial, and swirl velocities was determined for the same vane angle settings used in the radial traverses. The measurements were taken at a constant radial position of $r/D = 0.179$, which, in most cases, illustrates adequately the azimuthal flow variation. Measurements in each case spanned an angle of 48 deg, somewhat more than the 36 deg between successive blades. The variations in all normalized velocity components, u, v, and w, occurred in ~36-deg cycles, coinciding with the blade spacing. The profiles all showed significant variation with azimuthal position, except for those in or near recirculation zones, where the w-velocity component is dominant. These variations can be attributed to several causes, among them being blade stall from using flat blades at high angles of attack and wakes from blunt trailing edges.

Swirl Strengths

Swirl numbers S and S' were calculated from Eqs. (1) and (4), with the turbulent stress terms omitted. Measured velocities and pressure (with reference pressure p_∞ being at the outer edge of the swirler at $r/D = 0.25$), from the radial traverses, were used with appropriate numerical integration. Results are shown in Table 1, where the flat-blade swirler exhibits asymptotic behavior in its ability to produce strong swirl. Also shown is the measured ratio w_{m0}/u_{m0} for each swirl vane angle, where these represent the maximum values of swirl velocity w and axial velocity u measured in the radial traverse at the $x = 0$ location at the exit from the downstream plane of the swirler.

Conclusions

Measurements of actual swirler exit velocity profiles were made for swirl vane angles $\phi = 0$, 38, 45, 60, and 70 deg, using a five-hole pitot probe technique. These data form a useful part of a database for the evaluation of flowfield prediction codes and turbulence models, where the use of realistic inlet stream values of all three velocity components is needed rather than the use of unrealistic simple expressions. Assumptions of flat axial and swirl profiles with radial velocity equal to zero were found to be progressively less realistic as the swirler blade angle increases. Axial and swirl velocities peak strongly at the outer edges of the swirler exit, and significant nonzero radial velocities are present. Nonaxisymmetry is present in all swirl cases investigated.

References

[1]Beer, J. M., and Chigier, N. A., *Combustion Aerodynamics*, Applied Science Publishers, London, 1972.

[2]Khalil, E. E., *Modeling of Furnaces and Combustors*, Abacus Press, Tunbridge Wells, England, UK, 1982.

[3]Gupta, A. K., Lilley, D. G., and Syred, N., *Swirl Flows*, Abacus Press, Tunbridge Wells, England, UK, 1984.

[4]Gupta, A. K., and Lilley, D. G., *Flowfield Modeling and Diagnostics*, Abacus Press, Tunbridge Wells, England, UK, 1985.

[5]Chomiak, J., *Combustion: A Study in Theory, Fact and Application*, Abacus Press/Gordon and Breach, New York, 1990.

[6]Chigier, N. A., *Combustion Measurements*, Hemisphere, New York, 1991.

[7]Keating, E. L., *Applied Combustion*, Marcel Dekker, New York, 1993.

[8]Lilley, D. G., "Swirling Flows in Typical Combustor Geometries," *Journal of Propulsion and Power*, Vol. 2, No. 1, 1986, pp. 64–72;

also NASA CR-3869, Feb. 1985.

[9]Lilley, D. G., "Lateral Jet Injection into Typical Combustor Flowfields," NASA CR-3997, July 1986.

[10]Kerr, N. M., and Fraser, D., "Swirl. Part I: Effect on Axisymmetrical Turbulent Jets," *Journal of the Institute of Fuel*, Vol. 38, Dec. 1965, pp. 519–526.

[11]Mathur, M. L., and MacCallum, N. R. L., "Swirling Air Jets Issuing from Vane Swirlers. Part I: Free Jets; Part II: Enclosed Jets," *Journal of the Institute of Fuel*, Vol. 40, May 1967, pp. 214–245.

[12]Chigier, N. A., and Chervinsky, A., "Experimental Investigation of Swirling Vortex Motion in Jets," *Journal of Applied Mechanics*, Vol. 34, June 1967, pp. 443–451.

[13]Beltagui, S. A., and MacCallum, N. R. L., "Aerodynamics of Vane-Swirled Flames in Furnaces," *Journal of the Institute of Fuel*, Vol. 49, Dec. 1976, pp. 183–193.

[14]Sander, G. F., "Axial Vane-Type Swirler Performance Characteristics," M.S. Thesis, School of Mechanical and Aerospace Engineering, Oklahoma State Univ., Stillwater, OK, May 1983.

[15]Rhode, D. L., Lilley, D. G., and McLaughlin, D. K., "On the Prediction of Swirling Flowfields Found in Axisymmetric Combustor Geometries," *Journal of Fluids Engineering*, Vol. 104, 1982, pp. 378–384.

[16]Abujelala, M. T., and Lilley, D. G., "Swirler Performance and Confined Swirling Flow Predictions," *ASME Computers in Engineering Conference*, American Society of Mechanical Engineers, New York, 1984, pp. 233–241.